Nanoscale

CrossMark
← click for updates

Chirality-dependent densities of carbon nanotubes by *in situ* 2D fluorescence-excitation and Raman characterisation in a density gradient after ultracentrifugation†

Sofie Cambré, Pieter Muyshondt, Remi Federicci and Wim Wenseleers*

Density gradient ultracentrifugation (DGU) becomes increasingly important for the sorting of nano-materials according to the particles' density, hence structure and dimensions, which determine their unique properties, but the further development of this separation technique is hindered by the limited precision with which the densities could be characterized. In this work, we determine these densities by position-dependent 2D wavelength-dependent IR fluorescence-excitation and resonant Raman spectroscopy measured directly in the density gradient after ultracentrifugation. We apply this method to study the diameter and chirality-dependent sorting of empty and water-filled single-walled carbon nanotubes coated with two different surfactants, sodium cholate (SC) and sodium deoxycholate (DOC). The results elucidate the long standing contradiction that SC would provide better diameter sorting, while DOC is the most efficient surfactant to solubilise the nanotubes. A more predictable separation is obtained for empty DOC-coated nanotubes since their density is found to vary very smoothly with diameter. The accurate and chirality-dependent densities furthermore provide information on the surfactant coating, which is also important for other separation techniques, and allow to determine the mass percentage of water encapsulated inside the nanotubes.

Introduction

The unique and remarkably diverse electronic and optical properties of nanomaterials depend critically on their specific size and shape, even if their chemical structure is very similar.[1–3] A well-known prototypical example is single-walled carbon nanotubes (SWCNTs),[2,4] consisting of a rolled-up graphene sheet with diameters of 0.5 nm up to a few nm and typical lengths of a few microns. Their electronic and optical properties are critically dependent on their exact diameter and chiral structure (uniquely described by the chiral indices (n,m) of the so-called roll-up vector of the graphene sheet).[2] The lack of control in their synthesis, producing inhomogeneous mixtures of different diameters/chiralities, band gaps, *etc.*, has created a huge need for specialized separation and purification methods, as well as dedicated characterisation methods to distinguish species based on their structure and size dependent properties.

While originally developed for the separation of bio- and other macromolecules,[5] in recent years density gradient ultra-centrifugation (DGU) is booming as a very versatile and generally applicable tool for nanomaterials research.[6–9] Particles with different size or shape can be separated based on their different sedimentation rate (*i.e.* rate zonal ultracentrifugation), and/or based on their difference in buoyant density in isopycnic DGU.[8] The buoyant density, the key parameter for these isopycnic separations, not only depends on the exact size and shape of the nanomaterials, but also on the structure of the adsorbed dispersant layer.

Since the pioneering work of the Hersam group,[6] DGU has emerged as one of the most widely used and versatile techniques for the sorting of CNTs by diameter/chirality,[6,10] length,[11] electronic structure,[6] number of walls,[12] filling state,[13,14] and even enantiomers can be separated.[15] Pure solutions (>99%) of semiconducting or metallic tubes are already commercially available and single-chirality dispersions are achievable at laboratory scale for particular chiralities.[10] DGU has furthermore shown to be efficient for the sorting of graphene and other 2D materials according to the number of layers[7,16] and the sorting of metallic nanoparticles according to their specific size.[8,9]

In spite of these very nice demonstrations of the separation of carbon nanotubes (and other nanomaterials), the separation

mechanisms are not yet well understood, and various parameters are not yet optimised, which makes it impossible to predict and control the separations.

Analytical ultracentrifugation (AUC) could be very helpful in this perspective;[9,17,18] but analytical ultracentrifuges are limited to UV-VIS spectroscopy and refractive index measurements, which is insufficiently selective to distinguish individual CNT species in a polydisperse sample. A tedious workaround for this problem has recently been proposed, by first obtaining length-sorted single-chirality (6,5) solutions and using these as starting point for the analytical centrifugation,[18] thus, however, only yielding the density of one single chirality at a time. It is of course much more important to understand and control the differences in densities between different chiralities, as these determine the possibility to separate SWCNT chiralities (or other nanomaterials) from each other.

We have previously obtained such information, *i.e.* buoyant density as a function of SWCNT diameter and chiral structure, by manually selecting different fractions from the centrifuge tube and measuring extensive wavelength-dependent resonant Raman (RRS) and fluorescence-excitation (PLE) spectra of these separated fractions.[13] Such measurements are however extremely time consuming, too, and result in large error bars on the density determination due to the minimal volume of the discrete, manually selected fractions. General trends of the density–diameter relation could be obtained, but, to determine, understand and eventually control the density of different chiralities, a higher density-resolution is indispensable.

Ghosh *et al.*[10] proposed to perform fluorescence experiments (with a single laser excitation) as a function of height, *in situ* in the centrifuge tube, immediately after centrifugation, thus directly obtaining the density variation for a small subset of SWCNTs (those in resonance with the laser excitation). In this work, we show that the full position-dependent composition of the centrifuge tube after DGU can be characterized by the combination of a dedicated ultrasensitive wavelength-dependent IR fluorescence-excitation (PLE) and a resonant Raman scattering (RRS) spectrometer, both equipped with an automated translation stage.

We demonstrate the efficiency and importance of this new method, by comparing two well-known surfactants, sodium cholate (SC) and sodium deoxycholate (DOC) in their ability to sort SWCNTs by diameter. Previously, we have found that both of these bile salt surfactants are extremely efficient in solubilising SWCNTs,[19] without the use of sonication, therefore resulting in a high concentration of individually isolated intact SWCNTs in solution. These surfactants furthermore provide a very homogeneous, non-perturbing surrounding for the SWCNTs, as exemplified by the high resolution in optical spectroscopy and the long-term stability of the solutions (>10 years). While only distinct in one hydroxyl-group, these surfactants have been shown to behave quite differently in DGU separations. While DOC provides a better solubilisation,[19] the best DGU chirality separations are surprisingly obtained with SC.[6,10,13,20] The *in situ* characterisation helps in elucidating this long-standing contradiction.

Experimental details

Sample preparation

Sodium deoxycholate (DOC, also referred to as SDC in the literature, 99%) and sodium cholate (SC, 99%) were purchased from Acros organics. Raw SWCNTs from two different synthesis methods, high Pressure CO conversion[21] (HiPco from CNI, batch R0495C) and arc-discharge synthesis[22] (ARC from Nanoledge, batch P00508D) with typical lengths of the original, raw material ranging from ~100–1000 nm (suppliers specifications), were solubilized (10 mg/3 mL) in a 1% w/v surfactant solution in D_2O (Cortecnet, 99.89%), using only gentle stirring for 3 weeks (no sonication, as sonication would result in a much larger fraction of opened and thus water-filled SWCNTs[23]).

The so-obtained solutions were centrifuged for 24 hours at 16 215g (Sigma 2-16KCH centrifuge with swing-out rotor, 14 000 rpm), and the supernatant was collected for further sorting. This first medium speed 'pre-centrifugation' is based on sedimentation rate rather than density, to sediment out nanotube aggregates and bundles and end up with individually isolated SWCNTs in solution, and is particularly useful for the *in situ* experiments, where background absorption due to such impurities would otherwise limit signal strengths.

The density gradient medium used throughout this study is iohexol (tradename 'NycoDenz', obtained from Axis-shield in powder form), a monomeric analogue of the more commonly used dimer iodixanol.[6] While similar densities can be achieved, the lower molecular weight of iohexol makes it less sensitive to redistribution under the influence of the centrifugal field – a common limitation in maintaining shallow gradients during strong and/or prolonged ultracentrifugation. The higher density of D_2O allows the required density to be reached with lower mass-fractions of the gradient medium added, thereby further helping in creating more stable, shallow gradients.

Gradients were prepared in 1.3 mL (30 mm height) thinwall polyallomer centrifuge tubes, which are transparent in the visible and NIR. Starting from a step gradient (low density layer (700 μL of *e.g.* 1.15 g mL^{-1}) added gently on top of a higher density layer (600 μL of *e.g.* 1.27 g mL^{-1})), the centrifuge tube was tilted ~80° and rolled around its axis to form a continuous gradient. SWCNTs were added to both layers, to achieve a higher concentration for the *in situ* measurements. The density of both layers was slightly adapted between experiments to have the most important SWCNT bands located in the center part of the centrifuge tube (see below). The surfactant concentration in both layers of the step gradient was brought to 2% w/v. We initially chose this relatively high surfactant concentration (also used in some previous work[13,17,24]) as a precaution to avoid reaggregation during centrifugation.

Centrifugation was performed at 20 °C, for 48 h at 28 000 rpm (122 000g max) using a swing-out rotor (Kontron Centrikon T-1080, rotor TST 28). Visually no difference could be observed between 24 h and 48 h centrifugation runs, therefore we chose 48 h centrifugation times to be sure that the SWCNTs have reached their isopycnic point within very close approximation.

Experimental setups

Absorption spectra were collected using a Varian Cary 5E UV-VIS-IR spectrometer in the range of 200–2500 nm, using a quartz microcell (60 μL) with a path length of 3 mm. The densities were determined by calibration of a specific vibrational overtone absorption peak of iohexol, at 2285 nm, against iohexol solutions of known concentration and density (determined using a pycnometer) and corrected for small amounts of H_2O in D_2O (see ESI Fig. S1 and S3†).

Raman spectra were recorded in backscattering geometry using a Dilor XY800 triple spectrometer with liquid nitrogen cooled CCD detection. Several excitation wavelengths from different laser systems (Ar^+, Kr^+, tuneable Ti:sapphire lasers from Spectra-Physics models 2020, 2060 and 3900S, respectively) were used for resonant excitation in the optical transitions of different SWCNTs.

In order to obtain a high sensitivity over the full emission wavelength range of the SWCNTs, a high power pulsed Xe-lamp excitation (Edinburgh Instruments, custom adapted Xe900/XP920) was combined with a liquid-nitrogen cooled extended InGaAs photodiode array detector (Princeton Instruments OMAV:1024/LN-2.2), sensitive up to 2.2 μm. Spectra were corrected for detector and spectrograph efficiency, emission filter transparency, and (temporal and spectral) variations of the excitation light intensity using a reference detector measuring the intensity of each lamp pulse. *In situ* experiments were performed by mounting an automated translation stage in the sample chamber of the Raman and PLE setups. A horizontal strip of excitation light was achieved by using a cylindrical lens (in RRS) or by exploiting the combination of a horizontal image of the excitation spectrometer slit with a limited probe volume determined by the emission spectrometer slit (in PLE).

A single 2D PLE map was acquired in 10–15 min, with 5 nm excitation wavelength steps (~60 different excitation wavelengths per map) and an instrumental resolution of ~8 nm in excitation and ~15 nm in emission wavelength, resulting in a spatial resolution of 230 μm. Typical 1D RRS spectra (single excitation wavelength) were acquired in ~1–5 min, with sub-wavenumber spectral resolution and a spatial resolution of ~200 μm. Typically, the 2D+1 PLE maps were acquired with 1 mm steps in height, while the 1D+1 RRS spectra were acquired with 0.1 or 0.5 mm steps (where the +1 indicates the height dimension); and the height range was adjusted for each experiment taking into account that measurements needed to be performed before significant diffusion takes place. However, due to the large aspect ratio of SWCNTs, diffusion is quite slow as exemplified in Fig. S4, ESI.† Within the typical 6–10 hour time-frame after DGU, necessary to complete all experiments on one sample (strongly depending on the specific range of excitation wavelengths), a maximum error in density of only 0.002 g mL^{-1} can be expected.

Density calibration

To be able to determine the density of the SWCNTs after isopycnic DGU, the height in the centrifuge tube needs to be cali-

brated to the respective density. Typically, for each DGU run, 3–4 identical samples were prepared, so that RRS and PLE experiments could be acquired at the same time, *i.e.* in different centrifuge tubes; and from the other 1–2 samples we manually extracted well-defined 60–80 μL (~3 mm height) fractions using a syringe, to determine the density profile in the centrifuge tubes. Fractions were collected immediately after the DGU run, before diffusion of the gradient medium (which occurs much faster than diffusion of the nanotubes). The fractions were selected with 1–2 mm spacing between them, so that mixing with higher or lower density layers could be avoided (Fig. 1).

The density of the fractions was determined using the absorption of iohexol in the NIR (see ESI, Fig. S1†). When comparing the density profiles in two different centrifuge tubes of the same run, densities can be accurately reproduced in the central height range (5 to 25 mm; error <0.002 g mL^{-1}, see Fig. S3†), while for the top and bottom of the centrifuge tube the density varies much more steeply and larger deviations between different centrifuge tubes are obtained, of the order of 0.002–0.007 g mL^{-1}. Density ranges were therefore chosen in such a way that the most important SWCNT layers end up in this central height range. Fig. 1 presents a typical density-profile within the centrifuge tube after DGU. The data is fitted in the relevant height range using a polynomial.

To increase the diameter-range that can be studied in a single experiment, we mixed arc-discharge SWCNTs (d = 1.0–1.5 nm) and HiPco (d = 0.6–1.2 nm) solutions before the DGU-run. The density range was also chosen so that both empty and water-filled tubes,[13] of all these different chiralities, end up within the appropriate part of the centrifuge tube, where the accuracy of the density determination is the highest. Note that because of this broad diameter distribution (and
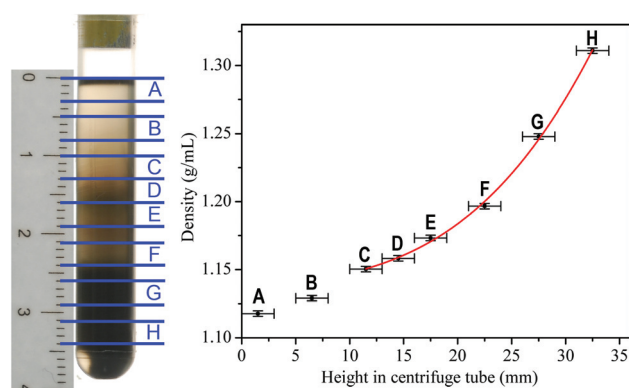
Fig. 1 Photograph of a centrifuge tube (left) containing a mixture of ARC and HiPco SWCNTs (2% w/v DOC) after centrifugation for 48 h at 122 000*g*. The selected fractions are indicated on the photograph, resulting in the density-profile shown on the right. The red curve represents a polynomial fit to the acquired data within the range of the *in situ* experiments. Fractions A and B don't contain any SWCNTs and are therefore not included in the fit. Fraction H contains mainly bundles of SWCNTs.
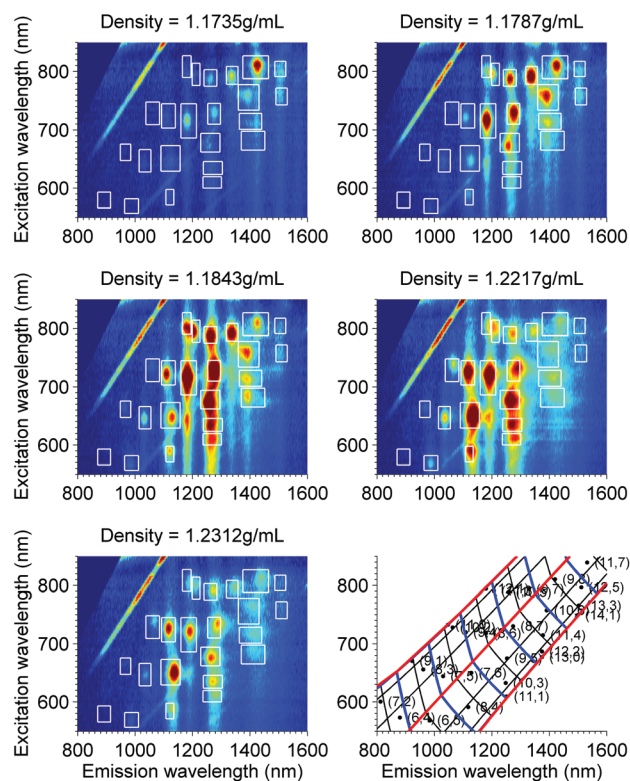
Fig. 2 Extracts from the 3D dataset, showing PLE plots obtained at different heights in the centrifuge tube. The white squares indicate the positions of the different chiralities, and the respective integration regions for obtaining their density profile (see text). The bottom right panel shows the diameter-chiral angle grid, with the red lines corresponding to lines of equal chiral angle (middle = chiral angle 0° and two outer lines are chiral angle 30°, with steps of 10°) and the blue lines are lines of constant diameter, with the spacing between the blue lines 0.1 nm. Predicted peak positions of empty individual chiralities are also given.[13]

steep gradient hence required), it is not possible to visually assess the diameter separation by the appearance of colours in the centrifuge tube (Fig. 1), but spectroscopically all chiralities can still be distinguished in this mixed sample.
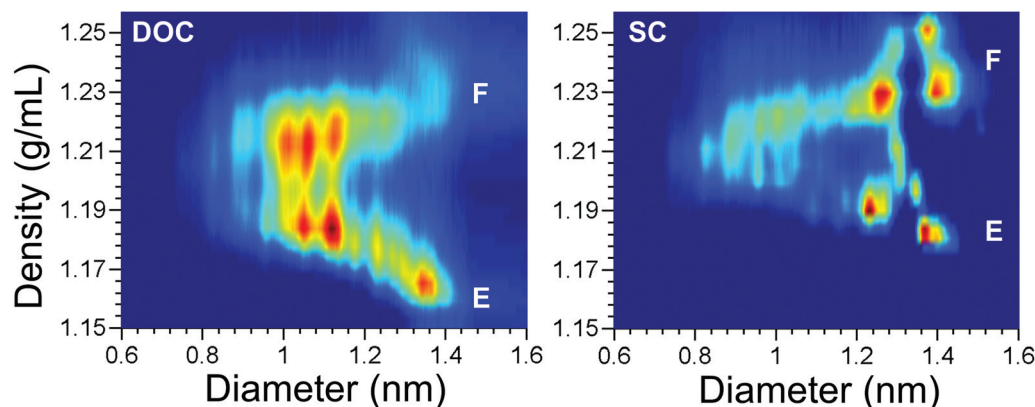
Results and discussion

PLE experiments

Fig. 2 presents a selection of PLE maps acquired at different heights in the centrifuge tube. As such a 3D dataset is obtained, *i.e.* intensity as a function of emission wavelength, excitation wavelength and height (or density) in the centrifuge tube. To extract the diameter/chirality-selective information from this 3D dataset, one can proceed in different ways.

A direct overview of the density as a function of diameter can be obtained by using our previously developed method to project the PLE maps on a diameter axis.[13] Based on the empirical relations for the electronic transition energies of semiconducting SWCNTs as a function of diameter and chiral angle of the nanotubes (first put forward by Bachilo *et al.*[25] and further adapted for empty SWCNTs solubilised with DOC in ref. 13), a grid of lines of constant diameter and constant chiral angle (presented in the bottom right panel in Fig. 2) can be obtained. The PLE spectra can then be integrated over strips of constant diameter, thereby reducing each 2D PLE map to a 1D dataset: fluorescence intensity *versus* diameter. As such, the 2D + 1 data set can be reduced to a 2D data set, as shown in Fig. 3.

Typically two branches are observed, corresponding to the empty (lower density branch, E) and water-filled (higher density branch, F) SWCNTs, and it can be directly observed that the empty and filled tubes in general sort in the opposite order, *i.e.* with the empty tubes having lower densities for larger diameters, as we previously found in ref. 13. A clear difference between SC- and DOC-coated SWCNTs can be immediately observed, which will be discussed further on.

To obtain a more detailed, chirality-dependent analysis of the sorting of the SWCNTs, the PLE maps can also be integrated over a fixed excitation and emission interval (white boxes in Fig. 2), including only a single PLE-peak, corresponding to one specific chirality. For larger diameters, where the electronic shifts due to water-filling become much larger and signals of filled tubes of one specific chirality might

Fig. 3 Projection of the PLE maps on diameter, as a function of density in the centrifuge tube for 2% w/v DOC (left) and 2% w/v SC (right), combining the data acquired for HiPco and arc-discharge SWCNTs. Lower density branch corresponds to the empty tubes (E) and the upper density branch to the water-filled (F) carbon nanotubes.
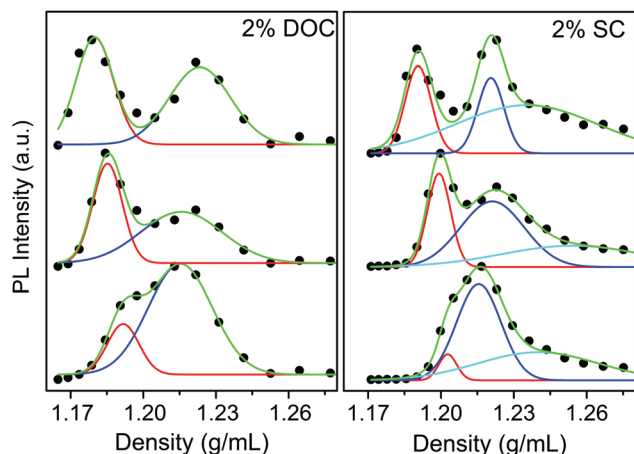
Fig. 4 PLE-intensity for different chiralities as a function of density in the centrifuge tube. From top to bottom: (9,8), (10,5) and (7,6). Fits are performed using a sum of Gaussians, corresponding to empty (red) and water-filled (blue) tubes. For the SC sample, due to the asymmetry of the bands, an additional Gaussian (cyan) is added to the fits, attributed to partially re-aggregated SWCNTs. An enlarged version can be found in the ESI, Fig. S2.†

overlap with empty tubes of a different chirality, separate integration regions for empty and filled tubes were used. As such a 1D data set is obtained for each chirality, *i.e.* intensity *versus* density, a representative selection of which is shown in Fig. 4.

When using DOC, two symmetric bands are observed for each chirality, corresponding to the empty (lower density) and water-filled (higher density) SWCNTs, which can each be fitted with a Gaussian. The bands remain resolved in density, even for relatively thin diameters (*e.g.* (7,6): $d = 0.88$ nm).

When using SC however, asymmetry in the bands is clearly observed, with a tail at higher density, most probably arising from partial reaggregation during the centrifugation. Large bundles can be found as a distinct band at much higher density. In Fig. 4 we fitted this asymmetry by adding an additional Gaussian band to the curve, accounting for the partially aggregated SWCNTs. For the smallest diameters, the density profiles of empty and filled tubes (red and blue curves in Fig. 4) strongly overlap and fitting results in large error bars on the determined densities. To solve this issue, we used RRS spectroscopy (see below).

Finally, the density profile of all the water-filled tubes is much broader than that of the empty tubes, which can be ascribed to the counteracting effects of gravity *versus* diffusion during the ultracentrifugation, where the pristine, empty and thus full-length SWCNTs will diffuse much less than the shorter, cut and therefore water-filled tubes.

RRS experiments

In addition to the PLE experiments, we also measure RRS spectra as a function of height in the centrifuge tube. With RRS only a subset of SWCNTs in resonance with the laser wavelength can be studied at a time, however also metallic SWCNTs can be studied and a higher spatial resolution can be achieved (laser *vs.* lamp excitation).

Fig. 5 presents the RRS spectra obtained at a laser excitation of 647.1 nm, in resonance with two ranges of SWCNTs, larger diameter metallic and smaller diameter semiconducting SWCNTs. Due to the high sensitivity of the RBM vibration for (external and internal) environment of the SWCNTs,[9,23,26,27] in combination with the high spectral resolution of the RRS spectrometer, the RBMs of empty and water-filled SWCNTs
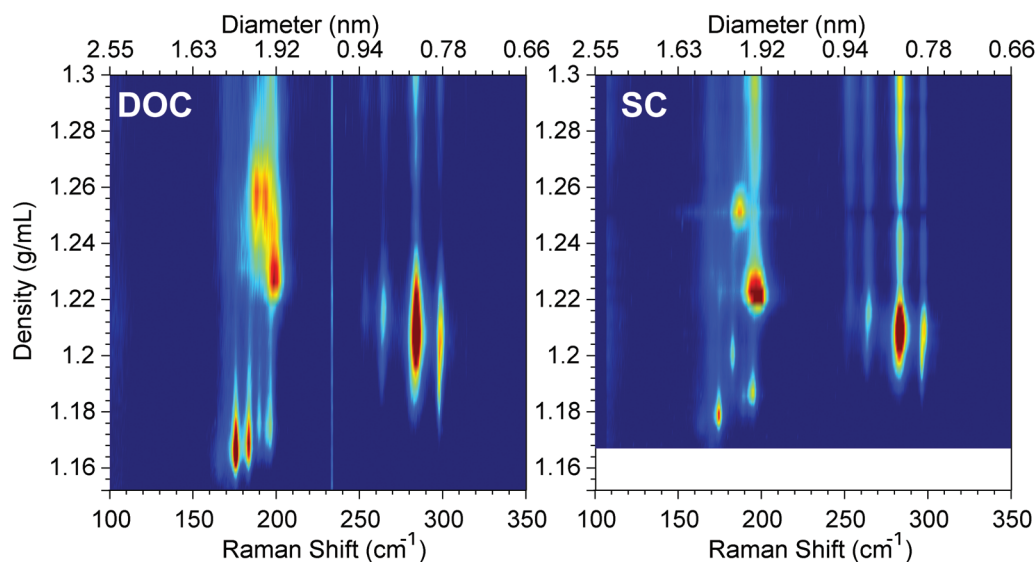
Fig. 5 RRS spectra excited at 647.1 nm as a function of density (height) for 2% w/v DOC (left panel) and SC (right panel). The fits of these experimental data as well as the RRS spectra excited at other excitation wavelengths can be found in the ESI.† (Note that in contrast to Fig. 3, the diameter increases to the left in this figure.)
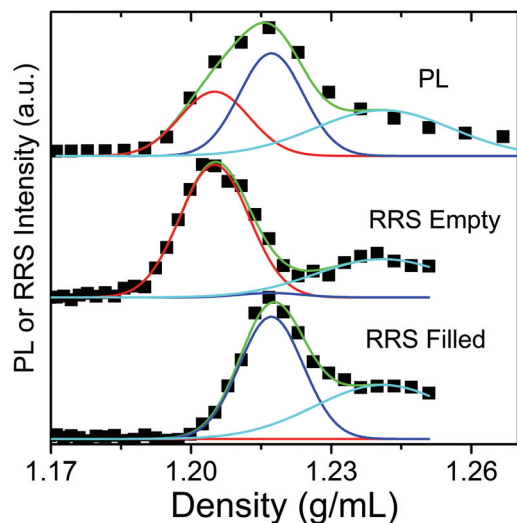
Fig. 6 Comparison of the density profiles of the (7,6) SWCNTs (2% w/v SC) obtained from the PLE measurements (*i.e.* bimodal distribution of empty and filled SWCNTs) and from the fits of the RRS spectra where empty and filled SWCNTs can be spectrally separated. Fits (green) are superpositions of 3 Gaussians, corresponding to empty (red), water-filled (blue) and an additional band for small aggregates that are formed during the centrifugation with SC (cyan). The 3 data sets were fitted simultaneously to achieve a better determination of the peak positions and line widths.

can be easily resolved spectrally, due to their shifted RBM vibration, and thus RRS allows obtaining the concentrations of empty and water-filled SWCNTs separately as a function of height in the centrifuge tube directly from the spectra, in contrast to the PLE experiments, where the position-dependent concentrations of empty and water-filled SWCNTs can only be determined by fitting the bimodal density-distribution. Since the RBMs of empty and water-filled SWCNTs partly overlap (shifts ~1–4 cm^{-1}) we fitted these 2D data sets using for each chirality two Lorentzians, corresponding to the empty and filled tubes, of which the line widths and peak positions are fitted simultaneously for all the different heights (densities), *i.e.* each spectrum is fitted with exactly the same line width and peak positions, only the amplitudes are allowed to vary (see Fig. S5–S8†). As such one obtains a very accurate determination of the RBM positions for the empty and the filled tubes, similarly as in previous work where different samples with different empty/filled compositions were fitted simultaneously.[23,26] It should be stressed that for these fits, only the spectra for densities smaller than 1.27 g mL^{-1} were selected, *i.e.* the density region of the isolated empty and filled tubes, thereby eliminating the densities where the bundles reside. These bundles have larger line widths than the individualized SWCNTs and are slightly red-shifted.[28] The advantage of spectrally resolving the empty and water-filled SWCNTs in RRS, is in particular important for the small diameter SWCNTs where the difference in density between empty and water-filled SWCNTs is very small. Fig. 6 gives the comparison of the PLE and RRS density profiles of the (7,6) SWCNTs (2% SC), from
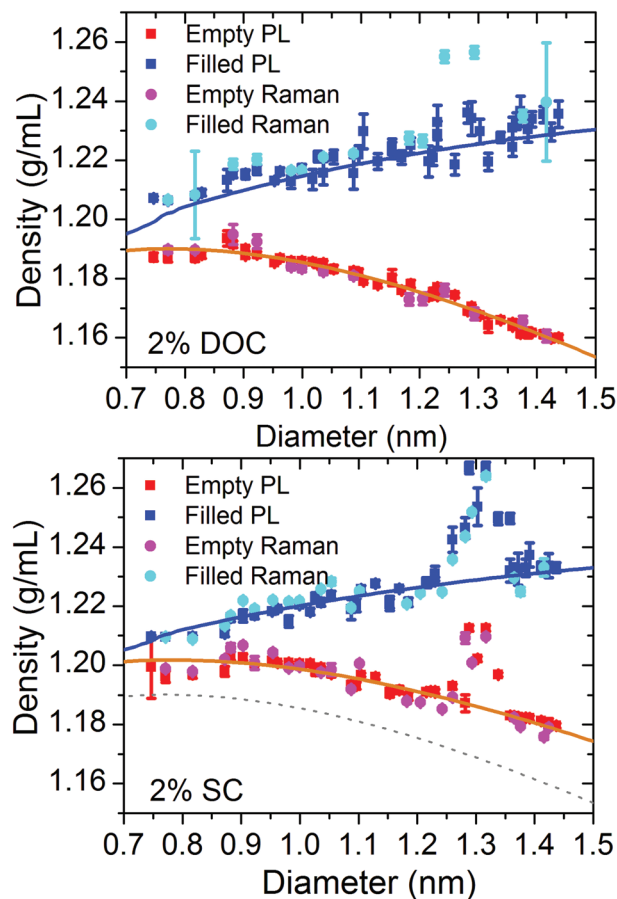
Fig. 7 Density *versus* diameter plots for empty (red, magenta) and water-filled (blue, cyan) SWCNTs obtained from PLE and RRS experiments, respectively. The orange solid lines represents a fit of the experimental data for the empty SWCNTs, using eqn (1) and fitting the thickness and density of the surfactant layer. The blue curve is calculated using the same thickness and density of the surfactant layer, and assuming a filling of the SWCNTs according to the hard sphere model from Picket *et al.*[29] and extended to larger diameters in ref. 13 (see text). For comparison, the model curve for empty DOC-coated SWCNTs is repeated in the bottom panel (gray dashed curve).
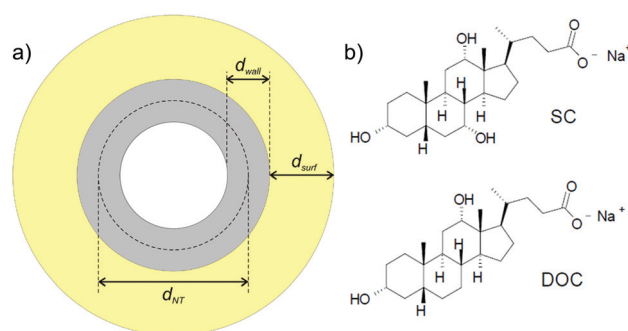
Fig. 8 (a) Geometrical model of a surfactant-coated SWCNT. The SWCNT has a diameter, d_{NT}, and a wall-thickness, d_{wall}. The surfactant-hydration layer is treated as a continuous concentric cylindrical shell, and has a thickness of d_{surf}. (b) Chemical structure of the SC and DOC surfactant.

which it is clear that RRS can be very helpful for a more accurate determination of the positions of empty and water-filled SWCNTs, if their density profiles partly overlap. In particular, by combining experiments and simultaneously fitting, the peak positions and line widths can be more accurately determined.

Combination of RRS and PLE

Far more precise than possible by manually extracting fractions, Fig. 7 presents an overview of the densities for all empty and filled SWCNT chiralities observed, combining the RRS and PLE experiments for 2% w/v DOC and SC. Data points are from the individual fits of the PLE and RRS data, thus some of the semiconducting tubes are presented twice in this plot. In total, densities of 50 (51) different empty and water-filled chiralities for DOC (SC) respectively, were determined of which the density–diameter dependence will be modelled in the next section.

Modelling of the surfactant layer

Three main differences can be observed between DOC and SC-dispersed SWCNTs (Fig. 7):

First of all, the densities of empty SC-wrapped SWCNTs are clearly higher than those of empty DOC-wrapped SWCNTs (both 2% w/v surfactant concentration; the higher buoyant density of SC-wrapped than DOC-wrapped tubes is also in good agreement with the AUC data reported by Fagan *et al.* for (6,5) SWCNTs with 1% surfactant, see Fig. 7 in ref. 18), and decrease less with diameter. To understand this difference, we introduce a simple geometric model for the buoyant density of SWCNTs (Fig. 8a), consisting of two concentric cylindrical shells, corresponding to the SWCNT wall and the surfactant-hydration layer surrounding the tube.[13,30] The buoyant density of SWCNTs can then be calculated as $\rho = M_{total}/V_{total}$ where V_{total} and M_{total} are the total volume and mass per unit length and

$$V_{total} = \pi(d_{NT} + d_{wall} + 2d_{surf})^2/4,$$

$$
\begin{aligned}
M_{total} = \pi/4[&\rho_{int}(d_{NT} - d_{wall})^2 \\
&+ \rho_{wall}((d_{NT} + d_{wall})^2 - (d_{NT} - d_{wall})^2) \\
&+ \rho_{surf}((d_{NT} + d_{wall} + 2d_{surf})^2 - (d_{NT} + d_{wall})^2)]
\end{aligned}
\tag{1}
$$

with d_{NT} the diameter of the SWCNT, which we calculated using the widely accepted C–C distance of 0.142 nm; d_{wall} and ρ_{wall} the thickness and density of the SWCNT wall, which we approximated by those of one graphite layer, *i.e.* $d_{wall} = 0.34$ nm and $\rho_{wall} = 2.23$ g mL^{-1} and ρ_{int} is the density of the SWCNT-cavity, which is either 0 for empty SWCNTs, or is determined by the density of the water inside the SWCNTs, which we will discuss later.

From the diameter dependence of the densities of the empty SWCNTs ($\rho_{int} = 0$), the thickness d_{surf} and the density ρ_{surf} of the surfactant – hydration layer can be obtained, by fitting the experimental data of the empty SWCNTs with eqn (1). We obtain $\rho_{surf} = 1.1068 \pm 0.0020$ g mL^{-1} and $d_{surf} = 1.152$

± 0.022 nm for the DOC-suspended SWCNTs, and $\rho_{surf} = 1.1444 \pm 0.0024$ g mL^{-1} and $d_{surf} = 1.453 \pm 0.046$ nm for the SC sample (section S5 in the ESI† discusses the error analysis for the fit parameters). Note that for the fit of the SC-suspended SWCNTs, the data points for $d = 1.26–1.35$ nm were not included as they show more complex behaviour that cannot be described by this simple model (with constant d_{surf} and ρ_{surf} for all chiralities, see below). The so-obtained fits are presented in Fig. 7 (orange curves). Note also that here, the surfactant layer (characterised by d_{surf} and ρ_{surf}) is defined as the concentric cylindrical volume around the SWCNT with different density compared to the surrounding bulk solution, and includes the surfactant molecules, but also the intercalated water molecules and empty spaces, and possibly a first hydration layer from which the gradient medium may be excluded, but not the much thicker hydration layer which has the same composition and density as the surrounding bulk solution (and which therefore does not change the buoyant density in isopycnic equilibrium). This is different from the parameter definitions used in the previous sedimentation rate based AUC analyses in ref. 17, 18, where the entire hydration layer of correlated molecules (even if of the same density as the bulk solution) adds to the friction experienced by the sedimenting tubes, and is thus included as a separate, much thicker layer of density equal to the surrounding solution density (there set to ~1 g mL^{-1}), while the surfactant layer is there defined as a much thinner equivalent volume containing only the anhydrous surfactant excluding the intercalated molecules or empty spaces between the flat SWCNT surface and surfactant molecules, based on the higher anhydrous surfactant density from literature. Thus, rate based separations yield more information on the hydration layer, while isopycnic separations yield a more precise determination of the density of the SWCNT–surfactant complex, as the density is less "diluted" by the very large hydration volume.

Secondly, the density difference between empty and water-filled SWCNTs is larger for the DOC-wrapped SWCNTs compared to the SC-wrapped SWCNTs, which is in fact in agreement with the thicker surfactant layer for SC (larger V_{total}) because:

$$\rho_{filled} - \rho_{empty} = \frac{m_{D_2O}}{V_{total}} \tag{2}$$

and it can be assumed that the mass of D$_2$O encapsulated inside the SWCNTs is not influenced by the externally adsorbed surfactants (with m_{D_2O} the mass of D$_2$O per unit length). This is further supported by the fact that the RBM and PLE shifts due to water-filling are nearly identical for DOC and SC-wrapped SWCNTs.

Knowing the thickness of the surfactant layer (and thus also V_{total}) determined above, we can thus extract the density of the encapsulated water, by using eqn (2). Fig. 9 presents the mass percentage of H$_2$O inside the SWCNTs (m_{H_2O}/m_{CNT}; stars and circles), obtained from the measured density difference between empty and filled SWCNTs (scaling from D$_2$O to H$_2$O was performed for easier comparison with literature data).
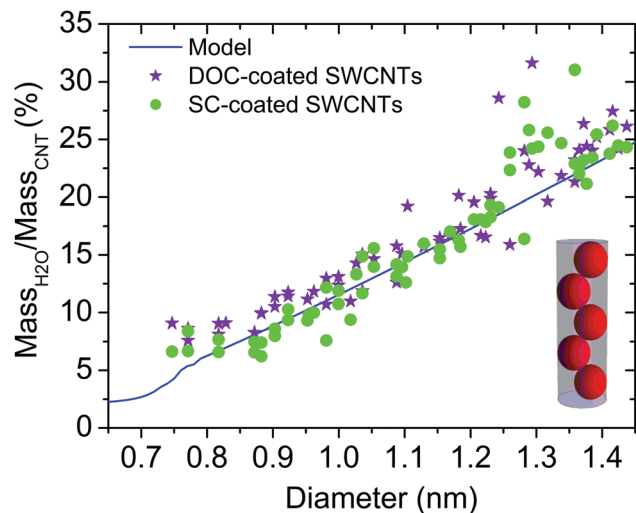
Fig. 9 Mass percentage of encapsulated water (H_2O) with respect to mass of SWCNT, as a function of diameter obtained from the experimental data for DOC-coated (purple stars) and SC-coated (green circles) SWCNTs. The blue curve represents a model where the water molecules are treated as hard spheres inside a cylinder, based on Picket et al.[29] as in ref. 13. The inset presents a side view of a SWCNT filled with such hard spheres. There is a very good agreement between the experimentally determined mass percentages and those obtained from the simple model.

These mass percentages are in very good agreement with predictions from molecular dynamics simulations (24–29 wt% for a (10,10) SWCNT, which has a diameter of 1.38 nm),[30–32] and with ensemble-averaged results from X-ray diffraction (a sample with a mean diameter of 1.41 nm yielded a mass percentage of 15.5% after 100 h of exposure to water vapour, but equilibrium was not yet fully reached).[33] Note that, as expected, the SC and DOC-suspended SWCNTs are found to be filled with the same amount of water (while based on very different d_{surf}), further demonstrating the consistency of the surfactant layer model.

The mass percentage of H_2O inside the SWCNTs can also be compared with a very simple model which we devised before,[13] where the water molecules are approximated by hard spheres and extrapolating the results from Picket et al.[29] describing the closest packing of such hard spheres inside a cylinder (blue curve in Fig. 9). As before,[13] the density of the spheres was set such that the bulk close packing of spheres (as obtained in the limit of large SWCNT diameters), yields the bulk density of water. However, for the diameter of the spheres we now used the core diameter of the (5,3) SWCNT (d_{water} = 0.208 nm), which is the smallest diameter SWCNT in which water-filling has been experimentally observed (and which is also close to the critical diameter for filling expected theoretically).[26] Details on the hard sphere model and the obtained internal water density are given in the ESI (section S6 and Fig. S10†). This model is in excellent agreement with the experimental data, perfectly reproducing the overall slope of

the mass percentage with diameter. This demonstrates that the filled SWCNTs are indeed entirely filled with densely packed water molecules. For comparison with the original data, we also inserted the water density of this hard-sphere model into eqn (1), to obtain the density of the water-filled SWCNTs, as shown in Fig. 7 (solid blue curves; note that no additional fit parameters are introduced to obtain these curves).

In addition to the general trend that is well described by the continuous model with concentric cylinders of constant d_{surf} and ρ_{surf}, the SC-wrapped SWCNTs also show pronounced oscillations in density, occurring at the same diameters for empty and filled tubes (Fig. 7, d = 1.26–1.35 nm), which arises from the packing of the discrete (and relatively large, semi-rigid) bile salt surfactant molecules on the SWCNT surface.

Such a sudden increase in SWCNT density (for SC-dispersed SWCNTs), would indicate either a decrease of the surfactant layer thickness by up to 35% (if the density ρ_{surf} remains the same), or an increase of its density by up to 2.7% (if the thickness of the surfactant layer remains constant). Our data for the empty tubes alone is not able to discriminate between both effects or a combination of both, but they already indicate that for certain chiralities a different packing of the surfactant molecules results in a sudden increase in density of the SWCNTs. However, the fact that the apparent mass fraction of encapsulated water in the water-filled tubes, as derived from eqn (2), deviates upward for these diameters around 1.3 nm (see Fig. 9), indicates that actually it is mainly the surfactant layer thickness (and thus V_{total} in eqn (2)) which is reduced for these particular SWCNT diameters. These fluctuations are most pronounced for the larger diameter (d = 1.26–1.35 nm) SC-coated SWCNTs, but most probably also induce the small deviations in density for the smallest diameter (d < 0.9 nm) DOC-coated water-filled SWCNTs (Fig. 7). Note that the only difference between SC and DOC is that the cholesterol group of SC bears three OH groups, all on the same side of the cholesterol group, whereas DOC has only two (see Fig. 8b). The three OH groups of SC divide the flattened, semi-rigid bean shape of the cholesterol group into a polar and apolar face, so that when adsorbed on the SWCNT it is very likely to adsorb with its apolar face flat onto the SWCNTs, thus creating a stacking which may or may not match with the circumference of the SWCNTs. Only when the packing matches with the SWCNTs' circumference, a compact (higher density, lower surfactant thickness) wrapping is possible, corresponding e.g. to the SWCNTs in the diameter range of d = 1.26–1.35 nm.

In contrast, for DOC, the two OH groups create only one polar edge, which may result in other orientations on the SWCNT surface, possibly tilted and partially overlapping, which would allow for a more flexible and gradual adaptation to different SWCNT diameters, explaining the absence of pronounced oscillations in the density–diameter relation for larger diameter DOC-coated SWCNTs. The less flexible SC-surfactant wrapping might also lie at the origin of the stronger aggregation observed for SC-coated SWCNTs during centrifugation.

While these fluctuations in density and thus different surfactant stackings aid in separating specific chiralities, and most likely lie at the basis of the excellent separations obtained with SC for small diameter SWCNTs,[6,10] the diameters at which they occur cannot be easily predicted. In contrast, DOC-coated SWCNTs show a more predictable density–diameter relation, becoming steeper for larger diameter empty SWCNTs, which is promising for extending the separations to larger diameters.

Conclusions

We have developed a new method to obtain rapid and very detailed chirality-dependent density-information from density gradient ultracentrifugation, by measuring full 2D PLE and RRS spectra as a function of height, directly in the centrifuge tube. We have demonstrated the importance of this method by comparing the isopycnic DGU sorting of empty and water-filled SWCNTs using two very similar surfactants, SC and DOC. The spectroscopic chirality selectivity enabling the simultaneous characterisation of a wide range of SWCNT diameters allows for deriving both surfactant layer thickness and density, in the assumption that these are constant, and moreover allows for deviations from this assumption for specific diameters to be recognized (e.g. indicating a reduced SC layer thickness for tube diameters of ~1.26–1.35 nm). The speed and ability to determine surfactant layer density (which instead had to be estimated from literature data on DOC in previous AUC work[17,18]) as well as thickness will make this technique particularly useful in systematic studies of the DGU separation parameters, in particular the choice of (co-)surfactant(s) and their concentrations, to improve the DGU separations of SWCNTs. While isopycnic separations yield high precision density measurements, rate based separations yield complementary information on the hydration layer,[17,18] not distinguishable by density. As sedimentation rate experiments can in principle also be performed with preparative centrifuges, by characterising the centrifuge tube after different, shorter centrifugation times (till now only performed by manual extraction or visual inspection[8,24]), one can also envisage the combination of such experiments with the present spectroscopic setup to simultaneously obtain chirality dependent information (however, for sedimentation experiments, the highest precision is still obtained on chirality- and preferably also length-sorted samples in AUC,[18] which remains time consuming). The extremely small structural difference between the two surfactant molecules, i.e. one additional hydroxylgroup for SC, has a drastic effect on the surfactant ordering around the SWCNTs, which results in qualitatively different DGU sorting behaviour. We have found that DOC-coated SWCNTs show a much smoother density–diameter relation, ascribed to a homogeneous coating that more flexibly adapts to different SWCNT diameters, in particular interesting for predictable and controllable diameter separations of larger diameter SWCNTs, while SC-coated SWCNTs show pronounced density oscillations which are interesting for separating specific chiralities.

Our results are not only important for the separation of SWCNTs by DGU, but will certainly also be useful for other separation methods that are governed by differences in the surfactant coating, such as gel chromatography[34] and the more recently introduced aqueous two-phase separation method.[35,36]

Notes and references

1 M. A. El-Sayed, Acc. Chem. Res., 2001, 34, 257.

2 A. Jorio, M. S. Dresselhaus and G. Dresselhaus, Carbon Nanotubes: Advanced Yopics in the Synthesis, Structure, Properties and Applications, Springer, 2008.

3 A. H. Castro Neto, F. Guinea, N. M. R. Peres, K. S. Novoselov and A. K. Geim, Rev. Mod. Phys., 2009, 81, 109.

4 S. Iijima and T. Ichihashi, Nature, 1993, 363, 603.

5 C. A. Price, Centrifugation in Density Gradients, Academic Press Inc, New York, 1982.

6 M. S. Arnold, A. A. Green, J. F. Hulvat, S. I. Stupp and M. C. Hersam, Nat. Nanotechnol., 2006, 1, 60.

7 A. A. Green and M. C. Hersam, Nano Lett., 2009, 9, 4031.

8 O. M. Bakr, V. Amendola, C. M. Aikens, W. Wenseleers, R. Li, L. Dal Negro, G. C. Schatz and F. Stellacci, Angew. Chem., Int. Ed., 2009, 121, 6035.

9 R. P. Carney, J. Y. Kim, H. Qian, R. Jin, H. Mehenni, F. Stellacci and O. M. Bakr, Nat. Commun., 2011, 2, 335.

10 S. Ghosh, S. M. Bachilo and R. B. Weisman, Nat. Nanotechnol., 2010, 5, 443.

11 J. A. Fagan, M. L. Becker, J. Chun and E. K. Hobbie, Adv. Mater., 2008, 20, 1609.

12 A. A. Green and M. C. Hersam, Nat. Nanotechnol., 2009, 4, 64.

13 S. Cambré and W. Wenseleers, Angew. Chem., Int. Ed., 2011, 50, 2764.

14 J. A. Fagan, J. Y. Huh, J. R. Simpson, J. L. Blackburn, J. M. Holt, B. A. Larsen and A. R. H. Walker, ACS Nano, 2011, 5, 3943.

15 A. A. Green, M. C. Duch and M. C. Hersam, Nano Res., 2009, 2, 69.

16 J. Kang, J.-W. T. Seo, D. Alducin, A. Ponce, M. J. Yacaman and M. C. Hersam, Nat. Commun., 2014, 5, 5478.

17 M. S. Arnold, J. Suntivich, S. I. Stupp and M. C. Hersam, ACS Nano, 2008, 2, 2291.

18 J. A. Fagan, M. Zheng, V. Rastogi, J. R. Simpson, C. Y. Khripin, C. A. S. Batista and A. R. H. Walker, *ACS Nano*, 2013, **7**, 3373.

19 W. Wenseleers, I. I. Vlasov, E. Goovaerts, E. D. Obraztsova, A. S. Lobach and A. Bouwen, *Adv. Funct. Mater.*, 2004, **14**, 1105.

20 F. Bonaccorso, T. Hasan, P. H. Tan, C. Sciascia, G. Privitera, G. Di Marco, P. G. Gucciardi and A. C. Ferrari, *J. Phys. Chem. C*, 2010, **114**, 17267.

21 M. J. Bronikowski, P. A. Willis, D. T. Colbert, K. A. Smith and R. E. Smalley, *J. Vac. Sci. Technol., A*, 2001, **19**, 1800.

22 C. Journet, W. K. Maser, P. Bernier, A. Loiseau, M. L. de la Chapelle, S. Lefrant, P. Deniard, R. Lee and J. E. Fischer, *Nature*, 1997, **388**, 756.

23 W. Wenseleers, S. Cambré, J. Čulin, A. Bouwen and E. Goovaerts, *Adv. Mater.*, 2007, **19**, 2274.

24 N. Nair, W.-J. Kim, R. D. Braatz and M. S. Strano, *Langmuir*, 2008, **24**, 1790.

25 S. M. Bachilo, M. S. Strano, C. Kittrell, R. H. Hauge, R. E. Smalley and R. B. Weisman, *Science*, 2002, **298**, 2361.

26 S. Cambré, B. Schoeters, S. Luyckx, E. Goovaerts and W. Wenseleers, *Phys. Rev. Lett.*, 2010, **104**, 207401.

27 S. Cambré, J. Campo, C. Beirnaert, C. Verlackt, P. Cool and W. Wenseleers, *Nat. Nanotechnol.*, 2015, **10**, 248.

28 M. J. O'Connell, S. Sivaram and S. K. Doorn, *Phys. Rev. B: Condens. Matter*, 2004, **69**, 235415.

29 G. T. Pickett, M. Gross and H. Okuyama, *Phys. Rev. Lett.*, 2000, **85**, 3652.

30 A. Quintilla, F. Hennrich, S. Lebedkin, M. M. Kappes and W. Wenzel, *Phys. Chem. Chem. Phys.*, 2010, 12.

31 A. Alexiadis and S. Kassinos, *Chem. Rev.*, 2008, **108**, 5014.

32 A. I. Kolesnikov, J.-M. Zanotti, C.-K. Loong, P. Thiyagarajan, A. P. Moravsky, R. O. Loutfy and C. J. Burnham, *Phys. Rev. Lett.*, 2004, **93**, 35503.

33 E. Paineau, P.-A. Albouy, S. Rouzière, A. Orecchini, S. Rols and P. Launois, *Nano Lett.*, 2013, **13**, 1751.

34 H. Liu, D. Nishide, T. Tanaka and H. Kataura, *Nat. Commun.*, 2011, **2**, 309.

35 J. A. Fagan, C. Y. Khripin, C. A. Silvera Batista, J. R. Simpson, E. H. Hároz, A. R. Hight Walker and M. Zheng, *Adv. Mater.*, 2014, **26**, 2800.

36 N. K. Subbaiyan, S. Cambré, A. N. G. Parra-Vasquez, E. H. Hároz, S. K. Doorn and J. G. Duque, *ACS Nano*, 2014, **8**, 1619.

Supplementary Information

Chirality-dependent densities of carbon nanotubes by in situ 2D fluorescence-excitation and Raman characterisation in a density gradient after ultracentrifugation.

Sofie Cambré, Pieter Muyshondt, Remi Federicci and Wim Wenseleers

1. <u>Density Calibration.</u>

To determine the density of the different fractions after DGU, we prepared well-calibrated solutions of a known density (determined using a pycnometer) and measured their absorption spectra. The gradient medium shows a characteristic absorption peak at 2285nm (well separated from the SWCNT absorption bands and another reason why D_2O is used instead of H_2O). Using the well-calibrated solutions of known density, the intensity of this absorption peak can be directly related to the density of the solutions.

The pycnometer was calibrated at a temperature of 20±0.3ºC using H_2O (ρ=0.9982±0.00013g/mL). As such, the density of the D_2O used was determined to be 1.10570±0.00015g/mL, and a 37.2% m/m Nycodenz solution in D_2O was found to have a density of 1.33579±0.00018g/mL.

Furthermore, the DGU also redistributes the H_2O-content (present as a minor impurity in the D_2O) in the different fractions. By measuring the absorption spectra of known concentrations of H_2O in D_2O, the H_2O-content in each fraction could be obtained and the densities were corrected for this.

For each of the SWCNT fractions, an absorption spectrum was measured and weighted reference spectra of Nycodenz and H_2O (with known concentration) were subtracted so that the characteristic absorption of the Nycodenz and H_2O disappears from the absorption spectrum (see Figure S1). The error on the concentration of Nycodenz and H_2O thus obtained results in a maximum error of 0.002g/mL on the densities.
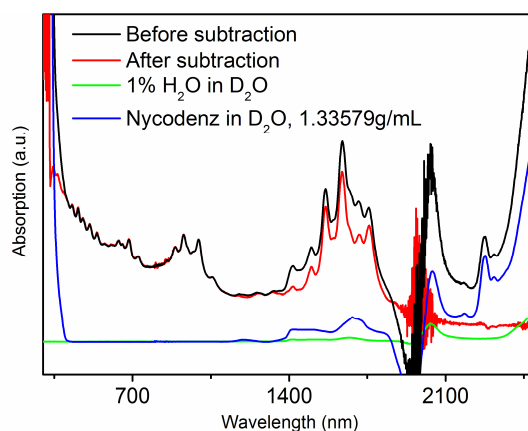
Figure S1: Absorption spectrum of an example SWCNT fraction obtained from the centrifuge tube after DGU (black) and the spectrum (red) after subtracting the weighted reference absorption spectra (those of H_2O (green) and Nycodenz (blue)), to eliminate their characteristic absorption bands. The absorption of pure D_2O was subtracted during the measurement. These specific amounts were then used to calculate the densities of each specific fraction.

To illustrate the relation of the obtained distributions as a function of density to the original data as a function of position in the centrifuge tube, we re-plot here Figure 4 from the main text, with a secondary axis denoting height (or depth) in the centrifuge tube on top (negative, relative to the liquid-air meniscus). It should be noted however, that, because of the slightly different gradients (height-to-density calibrations) used for the separation of DOC and SC-suspended SWCNTs, the height-scale cannot be directly compared between both experiments.
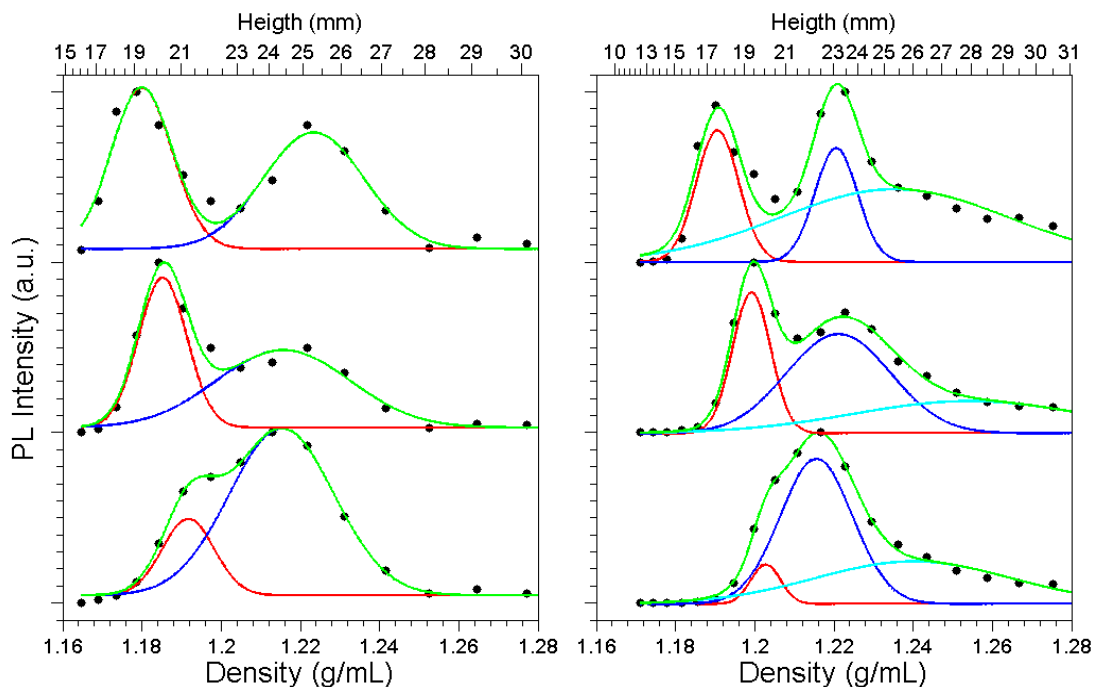
Figure S2: PLE intensity for different chiralities as a function of density (bottom axis) and height (top axis) in the centrifuge tube in 2% DOC (left panel) or 2% SC (right panel), From top to bottom: (9,8), (10,5) and (7,6). (See also Figure 4 in the main text).

2. Fraction selection

We prepared in each centrifuge run at least one reference sample, prepared identically in the other centrifuge tubes and manually selected fractions (~60-80µL) from these centrifuge tubes directly after the ultracentrifugation. The fractions were selected with 1-2mm distances between them so that densities of different fractions are not mixed. A typical example of a centrifuge tube after DGU and the selection of the fractions can be found in Figure 1.

Note that the densities are thus not determined inside the same DGU tube as the actual *in situ* measurements are performed. The reason for this is that the gradient medium diffuses at a much faster rate than the SWCNTs (smaller molecule) and therefore determining the densities after the *in situ* measurements would not give reliable results (see section 3).

To test the accuracy of the densities obtained in this way, i.e. including the accuracy of manually selecting the fractions, we prepared two reference samples and collected the fractions in the same way. Figure S2

presents the so-obtained density versus height curves, from which it is clear that within the relevant range of 5-25mm, densities are perfectly reproducible within the experimental error of 0.002g/mL, and therefore we aimed at separating the SWCNTs in this central region of the centrifuge tube. The top of the centrifuge tube (0 mm) and the bottom of the centrifuge tube (30 mm) deviate slightly (0.002 and 0.007g/mL in this specific example) since the density varies much more steeply in these particular regions. When fitting the density curve with a polynomial of degree 2, maximum deviations from the polynomial to the experimental data points are approx. 0.002g/mL. Therefore, measuring in the appropriate height region of the centrifuge tube (~5-25mm) and fitting the data points, we assume an accuracy of our density calibration of 0.002g/mL.
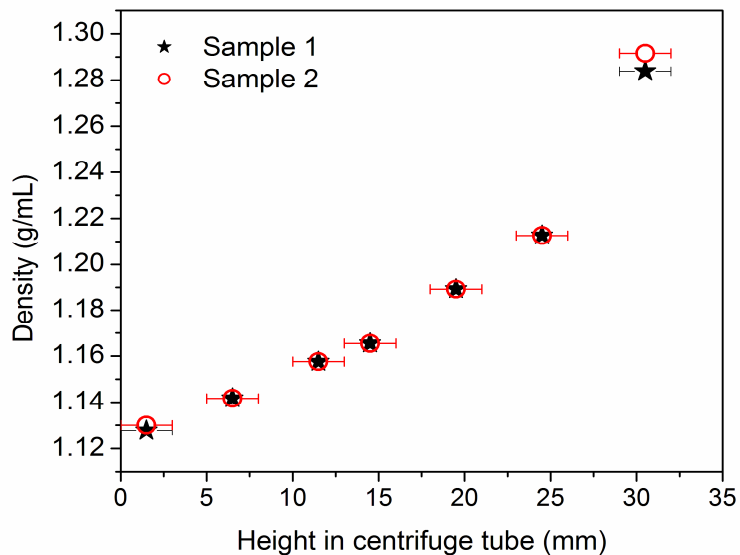
Figure S3: Densities of the different fractions (obtained from absorption) as a function of height in the centrifuge tube. A comparison is made between two different reference samples, presenting the reproducibility of the method.

3. Diffusion of the SWCNTs.

Time could be a very important factor for the *in situ* experiments. Immediately after the ultracentrifugation, diffusion of the SWCNTs is expected to destroy the separation. However, due to the large mass of SWCNTs their diffusion is very limited. To test this, we performed a RRS experiment (785nm) where we probe the position of empty and filled (9,7) tubes shortly after UCF (1 hour) and after leaving the sample diffuse for 24h. Slight diffusion can be observed as an increase of the Gaussian band width, but this is limited to only a 0.001g/mL shift in density after 24 hours. In addition, we observed a drift of all SWCNTs in the centrifuge tube, most probably due to creep of the plastic centrifuge tube after UCF (as it has expanded during UCF). However, the effect is extremely small (and constant for all SWCNTs), with only 0.004g/mL density shift after 24 hours.

Since experiments were performed in a time frame of maximum 6-10 hours after UCF, diffusion effects are thus minimal and within the experimentally determined error of 0.002g/mL. Diffusion of the gradient is much faster (smaller molecules) and therefore fractions for density calibration are collected immediately after each DGU run.
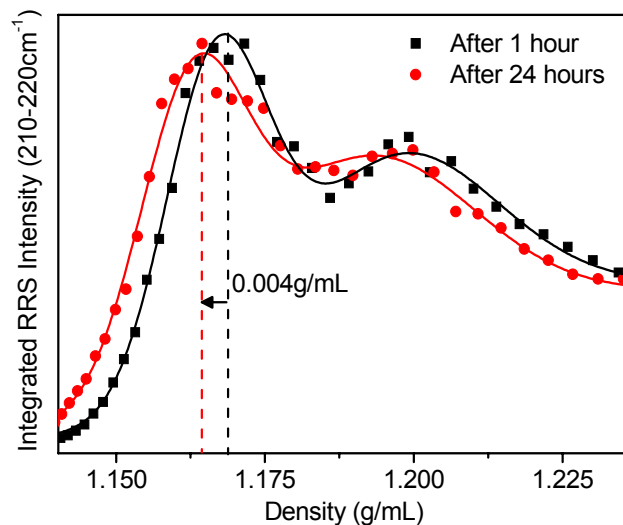
Figure S4: Integrated RRS intensity of a (9,7) SWCNT after separation (excitation wavelength = 785nm). The same spectrum (height) was acquired 1 hour and 25 hours after the ultracentrifugation. Diffusion of the SWCNTs leads to an increasing line width but is very slow: i.e. only a 0.001g/mL / 24 hours increase in Gaussian line width for the empty SWCNTs. We do observe a slight shift towards lower densities for all SWCNTs, which can be attributed to creep of the plastic centrifuge tube after ultracentrifugation, however this shift is very small, amounting to only 0.004g/mL after 24 hours.

4. *In situ* RRS experiments and fits at different excitation wavelengths

Unlike *in situ* PLE, i*n situ* RRS spectroscopy provides additional information on metallic SWCNTs, and those peculiar semiconducting SWCNTs that do not show fluorescence, *e.g.* the (5,3) chirality. Figures S4-S7 show a representative set of Raman data, measured at different excitation wavelengths (647.1nm, 785nm, 514.5nm and 725nm), in resonance with both metallic and semiconducting larger and smaller diameter SWCNTs.

The RRS data excited at 647.1nm are presented in two distinct regions, corresponding to larger diameter metallic SWCNTs (150-220cm^{-1}) and smaller diameter semiconducting SWCNTs (240-310cm^{-1}).

1D+1 RRS spectra were fitted using a combination of empty and filled peak positions for each chirality.

a)   647.1nm.
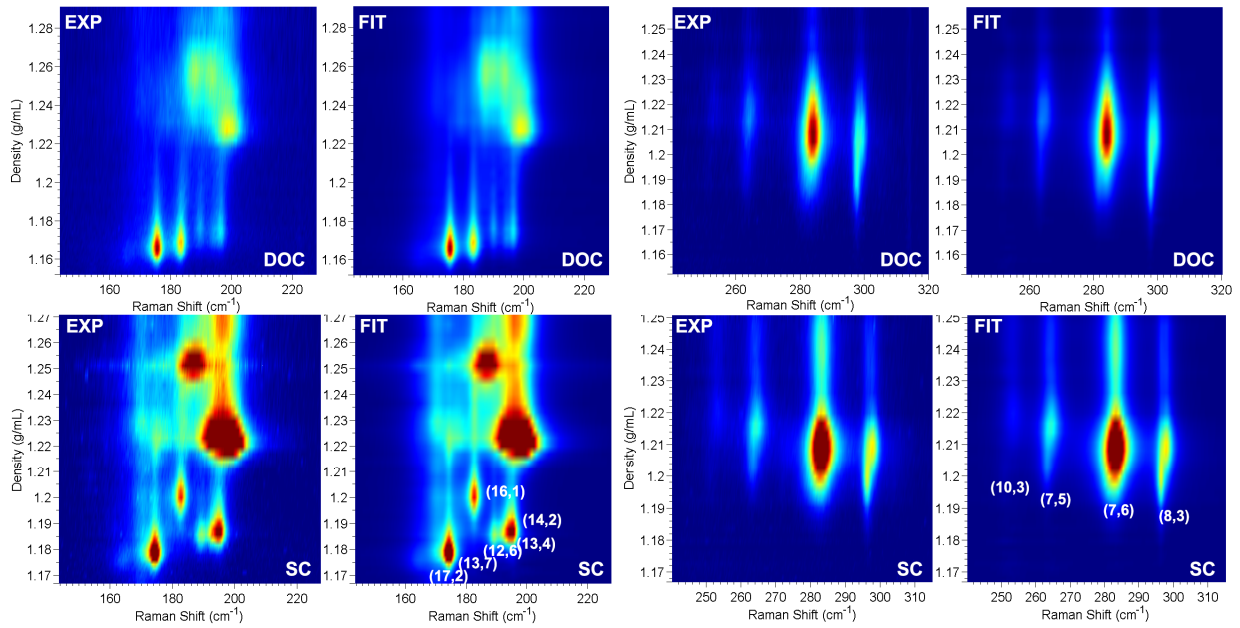
Figure S5: In situ RRS spectra and fits with excitation at 647.1nm, for 2% DOC (Top panels) and 2% SC (Bottom panels). Two distinct regions are fitted separately, corresponding to thicker and thinner diameter SWCNTs. From left to right the (17,2), (13,7), (16,1), (12,6), (13,4), (14,2), (10,3), (7,5), (7,6) and (8,3) tubes are fitted.

b) *785nm*
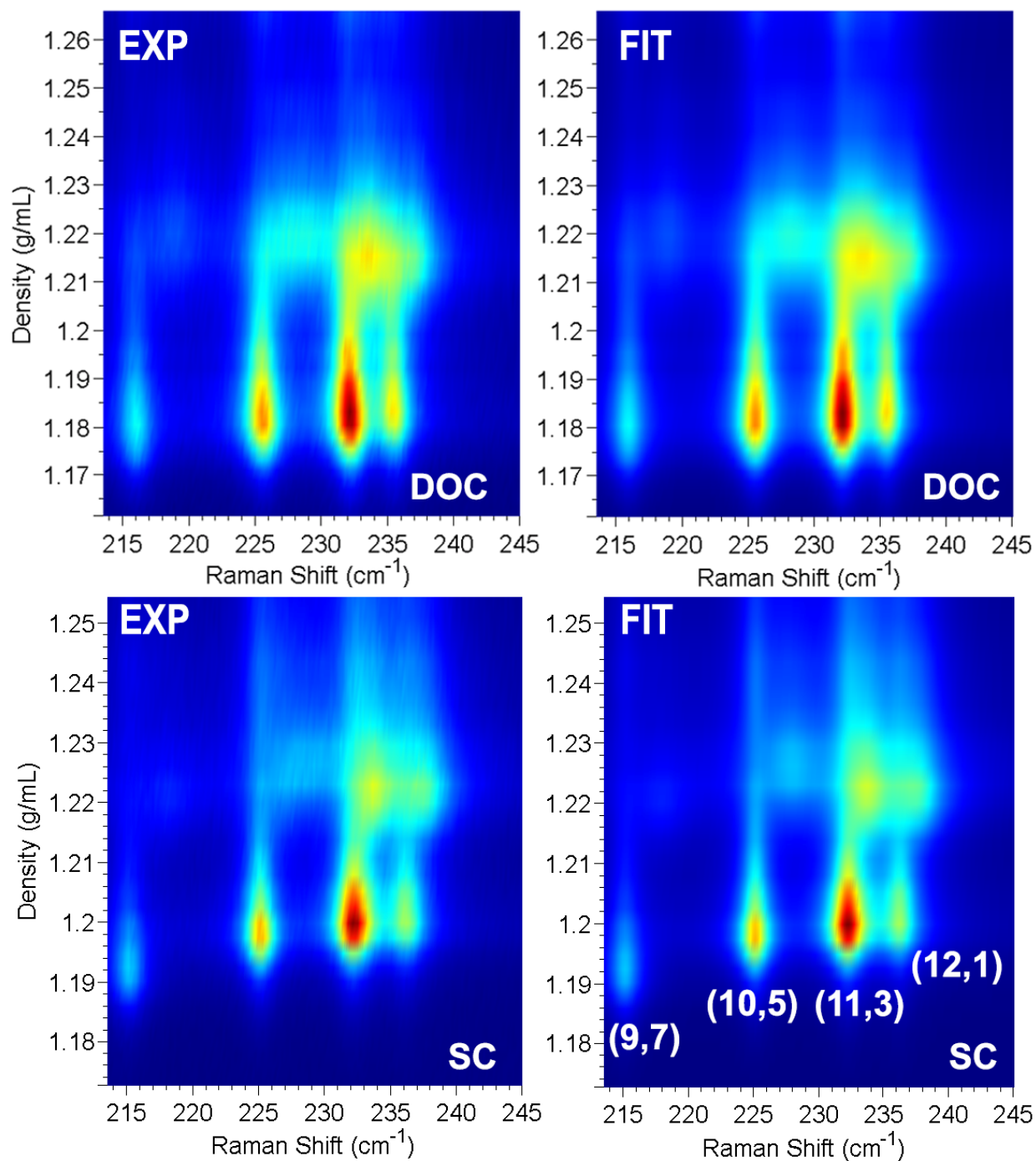
Figure S6: In situ RRS spectra and fits with excitation at 785nm, for 2% DOC (top panels) and 2% SC (bottom panels).. From left to right, the (9,7), (10,5), (11,3) and (12,1) tube are fitted

c) 514.5 nm
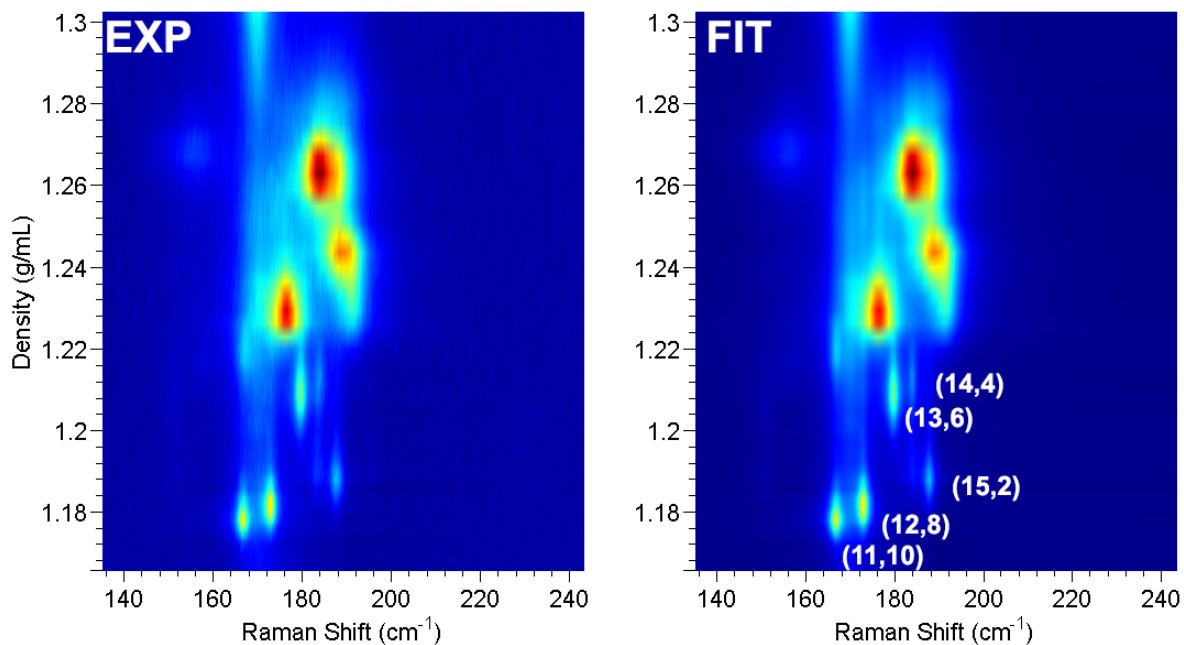
Figure S7: In situ RRS spectra (left) and fits (right) with excitation at 514.5 nm, for 2% SC. From left to right the (11,10), (12,8), (13,6), (14,4), (15,2) tubes.

d) 725 nm
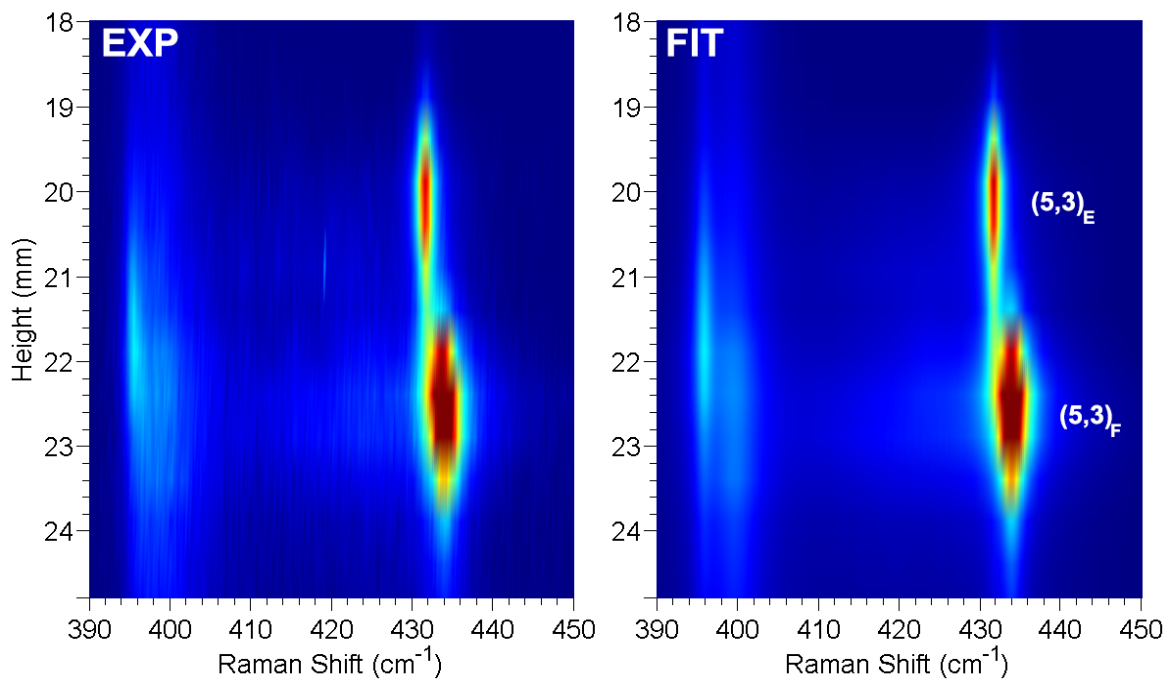
Figure S8: In situ RRS spectra (left) and fits (right) with excitation at 725nm, for 0.7% DOC, in resonance with the (5,3) tube. Also for this specific small diameter tube, empty (E) and filled (F) tubes can be clearly separated spectrally (as well as spatially) from each other.

5. Model fitting: Error analysis

The density and thickness of the surfactant layer that are determined by the model fit to the empty SWCNT densities (see Figure 7 and main text) are strongly correlated fit parameters, which needs to be taken into account to determine the error margins on these fit parameters, based on the full Jacobian of the χ^2. Therefore , we considered different approaches in deriving a properly defined χ^2: (1) One might simply weigh the experimental data points according to their respective experimental errors, yielding a χ^2-surface as presented by the blue contour plot in Figure S9. However, inspection of the fit (Figure 7) shows that the deviations due to chirality dependent variations of density (which are not included in the model) dominate over the actual experimental errors, so it is not appropriate to give undue additional weight to data points with smaller experimental errors. (2) The best estimate of density and thickness of the surfactant layer is thus rather obtained by giving the same weight to all data points. The green contours in Figure S9 show the resulting χ^2-surface when using a single, average experimental error. (3) To furthermore account for the systematic deviations due to the density variations for individual chiralities (not included in the concentric cylinder model, which only considers diameter), it is in this case more appropriate to normalize χ^2 based on these deviations rather than the *experimental* errors (red contours in Figure S9). The best fit values and correct (more conservative) error bars (1σ) which we have reported in the manuscript for density and thickness of the surfactant layer are thus determined by the last approach. Note however, that the alternative weighting schemes (albeit less appropriate) also yield fitted values within these conservative error bars.
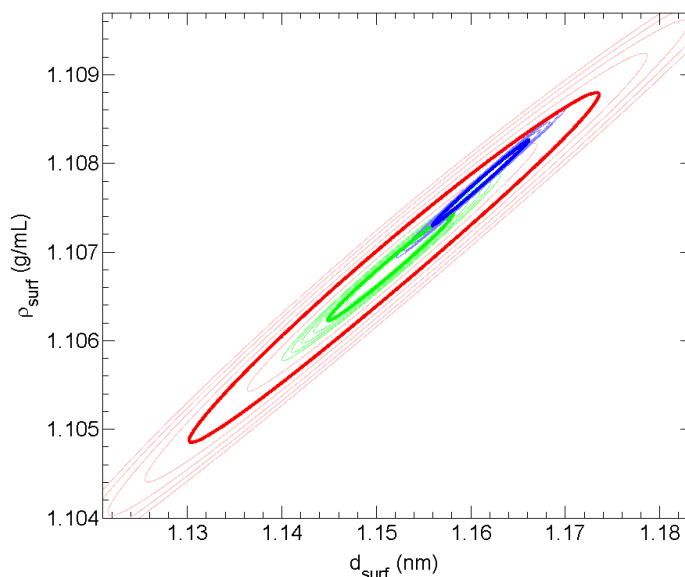
Figure S9. Contour plot of the χ^2 corresponding to the fit to the empty SWCNT data (orange curves in Figure 7). Contour lines are plotted at increments of 0.5 in χ^2, from the minimum χ^2 value (χ^2_{min}, i.e. best fit) up to χ^2_{min} +3, corresponding to 0.5σ through 3σ confidence levels on the fit parameters, with the 1σ contour represented by a bold curve. The colours represent the different weighting schemes considered (see text). The bold red curve corresponds to the 1σ error bars reported in the main text, and takes into account not only the experimental errors, but also the intrincic chirality dependent deviations from the simplified cylinder model (which is based on diameter only) which are larger.

6. Hard sphere model for the density of the encapsulated water

For the core density of the water-filled SWCNTs, we used the simple geometric model devised in reference 13, approximating the water molecules by hard spheres, closely packed in a hard cylinder, for which the analytical results by Pickett *et al.*[29] were used. For diameters larger than those for which analytical results have been obtained in reference [29], the volume fraction of the hard-sphere packing was extrapolated as $a+b/d$, such that at infinite diameter d, the volume fraction of a bulk close packing of spheres, $a=\pi/3\sqrt{2}$, is retrieved. Also as in reference [13], the density of the spheres was chosen such that this bulk close-packed arrangement corresponds to the density of bulk water, and the diameter of the cylinder was set to $d_{NT}-d_{wall}$, corresponding to the hollow core of the SWCNT. However, in reference [13], the diameter of the hard spheres was taken to be the distance between oxygen atoms in two water molecules connected by a hydrogen bond (d_{water}=0.29nm). That essentially described the longitudinal spacing of water molecules, but for describing the evolution of density with SWCNT diameter, it is rather the (lateral) size of the molecules (relative to the nanotube channel) which is more important. This size is smaller and known more precisely from the filling of small diameter tubes: water is experimentally known to enter thinner nanotubes down to the (5,3) SWCNT, with a diameter of 0.548nm and thus an inner core diameter of 0.208nm (and also theory predicts a critical diameter for filling close to this value).[26] We therefore now used this as a more accurate value for the effective sphere diameter (d_{water} =0.208nm). The resulting model density of the internal water as a function of SWCNT diameter (for both D$_2$O, as used here, and H$_2$O), is plotted in Figure S10.
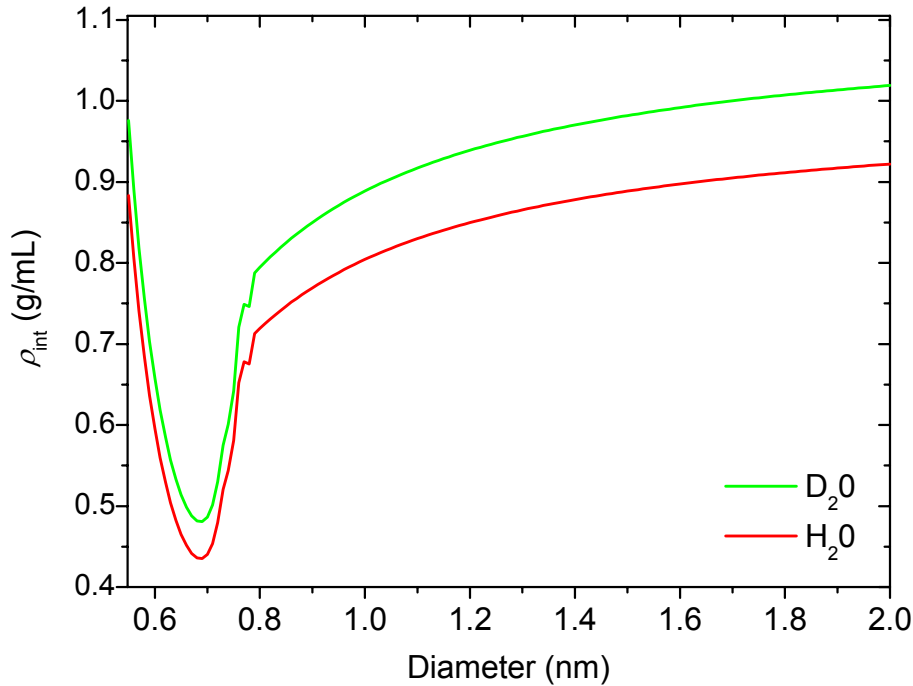
Figure S10. Density of the encapsulated water in water-filled SWCNTs as a function of SWCNT diameter, as calculated from the hard-spheres model using d_{water} =0.208nm (see text).